Rapid Diffusion-Weighted Magnetic Resonance Imaging of the Brain Without Susceptibility Artifacts

Single-Shot STEAM With Radial Undersampling and Iterative Reconstruction

Andreas Merrem, MSc, Sabine Hofer, PhD,* Dirk Voit, PhD,* K.-Dietmar Merboldt, PhD,* Jakob Klosowski, MSc,* Markus Untenberger, PhD,* Julius Fleischhammer, MD,† and Jens Frahm, PhD**

Objective: The aim of this study was to develop a rapid diffusion-weighted (DW) magnetic resonance imaging (MRI) technique for whole-brain studies without susceptibility artifacts and measuring times below 3 minutes.

Materials and Methods: The proposed method combines a DW spin-echo module with a single-shot stimulated echo acquisition mode MRI sequence. Previous deficiencies in image quality due to limited signal-to-noise ratio are compensated for (1) by radial undersampling to enhance the flip angle and thus the signal strength of stimulated echoes; (2) by defining the image reconstruction as a nonlinear inverse problem, which is solved by the iteratively regularized Gauss-Newton method; and (3) by denoising with use of a modified nonlocal means filter. The method was implemented on a 3 T MRI system (64-channel head coil, 80 mT · m gradients) and evaluated for 10 healthy subjects and 2 patients with an ischemic lesion and epidermoid cyst, respectively.

Results: High-quality mean DW images of the entire brain were obtained by acquiring 1 non-DW image and 6 DW images with different diffusion directions at b = 1000 s · mm. The achievable resolution for a total measuring time of 84 seconds was 1.5 mm in plane with a section thickness of 4 mm (55 sections). A measuring time of 168 seconds allowed for an in-plane resolution of 1.25 mm and a section thickness of 3 mm (54 sections). Apparent diffusion coefficient values were in agreement with literature data.

Conclusions: The proposed method for DW MRI offers immunity against susceptibility problems, high spatial resolution, adequate signal-to-noise ratio and clinically feasible scan times of less than 3 minutes for whole-brain studies. More extended clinical trials require accelerated computation and online reconstruction.

Key Words: diffusion-weighted MRI, radial sampling, iterative reconstruction, Gauss-Newton method

(*Invest Radiol* 2017;52: 428–433)

Diffusion-weighted (DW) magnetic resonance imaging (MRI) finds extensive clinical use in the diagnosis of stroke and neoplasms.[1] In contrast to applications serving fiber tractography, respective acquisition protocols usually comprise only a very limited number of diffusion directions for tensor definition. Moreover, they primarily aim at mean DW images and maps of the apparent diffusion coefficient (ADC) at sufficiently high resolution and with short measuring times. Such protocols should allow for a robust and sensitive detection of acute ischemic lesions and characterization of brain tumors. Oncologic applications of DW MRI even extend into other organ systems such as the liver, breast, and prostate.[1,2]

Received for publication November 1, 2016; and accepted for publication, after revision, January 5, 2017.

From the *Biomedizinische NMR Forschungs GmbH am Max-Planck-Institut für biophysikalische Chemie; and †Department of Neuroradiology, University Medical Center, Georg-August University, Göttingen, Germany.

The authors report no conflicts of interest.

Correspondence to: Andreas Merrem, MSc, Biomedizinische NMR Forschungs GmbH am Max-Planck-Institut für biophysikalische Chemie, Am Faßberg 11, 37077 Göttingen, Germany. E-mail: amerrem@gwdg.de.

ISSN: 0020-9996/17/5207–0428
DOI: 10.1097/RLI.0000000000000357

Although DW MRI is generally considered to be of high diagnostic value, the quality of current DW images is often compromised by artificial signal alterations and geometric distortions, which are caused by the use of an echo-planar imaging (EPI) readout sequence for a DW spin-echo signal.[3] EPI involves contributions from gradient echoes with long echo times that are sensitive to local magnetic field inhomogeneities. These problems are usually caused by susceptibility differences between tissues and air or venous blood, and therefore are unavoidable in many parts of the human body.

To overcome this dilemma, we previously proposed a DW MRI sequence that combines a DW spin echo with a signal readout by a high-speed stimulated echo acquisition mode (STEAM) sequence.[4,5] While the sensitivity to susceptibility problems completely vanishes, the method presented with much lower signal-to-noise ratio (SNR) compared with the EPI alternative as recently demonstrated for a comparative study of infratentorial ischemic stroke.[6] Here, we developed a modified acquisition and reconstruction strategy, which for the first time yields DW STEAM images of diagnostic quality in clinically feasible scan time. The new method uses a single-shot STEAM readout with radial encoding and pronounced undersampling and redefines the image reconstruction as a nonlinear inverse problem. While the first change enhances the flip angle of the STEAM readout pulses and thus improves the signal strength of corresponding stimulated echoes,[7,8] the iterative reconstruction jointly estimates the image and all coil sensitivities as previously proposed for real-time MRI.[9–11] This latter approach markedly improves the achievable image quality for highly undersampled data acquisitions. Moreover, whole-brain acquisitions with gapless coverage take advantage of another prior. The reconstruction problem of such multislice acquisitions benefits from a similarity constraint for the coil sensitivities from directly neighboring sections. In this work, it is shown that the resulting DW STEAM MRI technique allows for clinical whole-brain protocols of enhanced diagnostic quality (ie, adequate SNR and no susceptibility artifacts) within total measuring times of 1.5 to 3 minutes depending on spatial resolution.

MATERIALS AND METHODS

Magnetic Resonance Imaging

All studies were performed at 3 T using an MRI system with 80 mT · m^{-1} gradients (Magnetom Prisma; Siemens Healthcare, Erlangen, Germany). Whole-brain DW STEAM MRI was performed on 10 young subjects without known illness using the standard 64-channel head coil. Preliminary clinical trials included a patient with lacunar stroke and a patient with an epidermoid cyst. In all cases, written informed consent, according to the recommendations of the local ethics committee, was obtained before MRI.

Diffusion-weighted single-shot STEAM MRI was implemented as previously outlined,[5] but with 2 major modifications: (1) as shown in Figure 1, Cartesian phase-encoding with partial Fourier imaging was replaced by the use of highly undersampled radial trajectories homogeneously spanning 360 degrees of k-space; and (2) image reconstruction

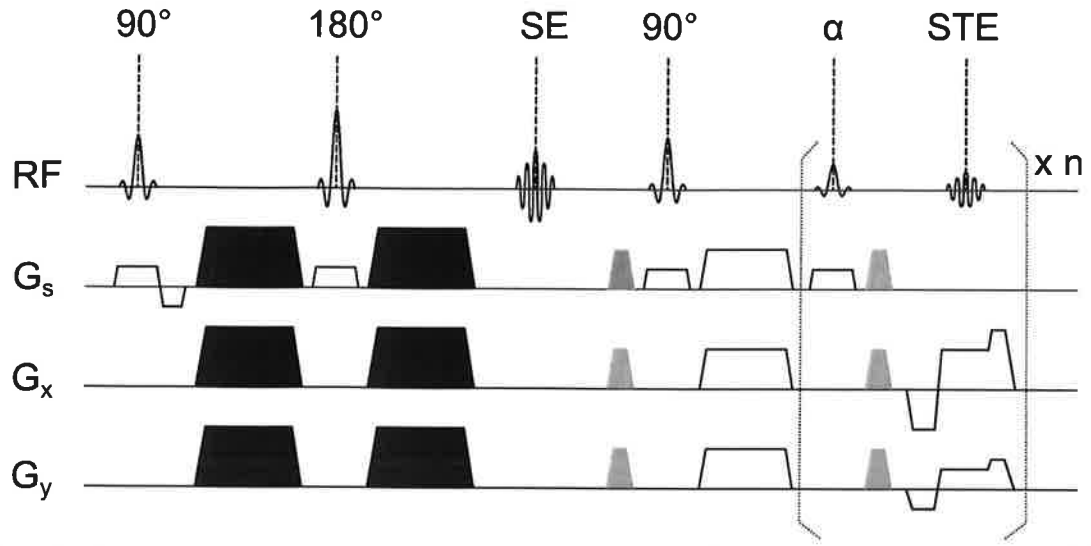

FIGURE 1. Diffusion-weighted STEAM MRI combines a DW spin-echo with a single-shot STEAM sequence using an undersampled radial trajectory. For details see text. Black, diffusion gradients; gray, spoiler gradients; G_s, slice-selection gradient; G_x, G_y, frequency-encoding gradients; SE, spin echo; STE, stimulated echo; RF, radiofrequency.

by Fourier transformation was replaced by nonlinear inversion (NLINV)[9–11] modified as described hereafter. For the readout pulses, the flip angles for successive stimulated echoes (ie, radial spokes) were calculated according to[4,5,12]

$$\alpha_i = \arctan(\sin\alpha_{i+1}\exp(-TR/T1))$$

with a T1 estimate of 800 milliseconds at 3 T. However, we used a flip angle of 40 degrees instead of 90 degrees for the last spoke. During experimental sequence optimization, this choice reduced residual streaking artifacts that resulted from a too-high stimulated echo intensity (ie, spoke in k-space).[13] On the other hand, the lower flip angle only led to a relative signal loss of less than 3%. Moreover, during the STEAM readout period the establishment of transverse coherences was avoided by FID spoiler gradients as indicated in Figure 1. The "inherent" diffusion weighting due to imaging and spoiler gradients corresponds to a value of $b \leq 30\ s \cdot mm^{-2}$, which is of no practical significance for clinical DW MRI of the brain. To suppress fat signal contributions from the scalp, a CHESS pulse[14] (not shown) was applied immediately before the sequence.

To cover the entire brain, multiple slices without gaps were acquired in an interleaved order. The total repetition time was set to 12 seconds to ensure a 6-second delay for the excitation of directly neighboring slices. Table 1 summarizes detailed acquisition parameters for 2 whole-brain protocols with $b = 1000\ s \cdot mm^{-2}$ and 6 diffusion gradient directions. The protocols either emphasize speed (ie, a measuring time of 84 seconds) at an in-plane resolution of 1.5 mm and a slice thickness of 4 mm ("fast DWI"), or high spatial resolution (ie, 1.25 mm in plane and 3 mm thickness) within 168 seconds ("high-resolution DWI").

Preprocessing

The proposed reconstruction method uses information from multiple receive coil elements as in parallel imaging. To reduce the computational load, the same channel compression technique was applied as previously implemented for real-time MRI.[9–11] It reduces the amount of raw data by introducing a smaller number of virtual channels obtained by a principal component analysis. Here, the calculation of the channel compression matrix was based on the data of all slices that are jointly reconstructed.

The radial data sets were further corrected for deviations from the intended k-space trajectory that are caused by imperfections of the gradient system. The applied gradient delay correction estimates and corrects for parallel shifts with respect to the realized radial traversal of k-space using a model described by Peters et al.[15] Subsequently, the radial data were interpolated onto a Cartesian grid without density

TABLE 1. Acquisition Parameters for Diffusion-Weighted Single-Shot STEAM MRI

	Fast DWI	High-Resolution DWI
Field of view, mm^2	192 × 192	190 × 190
Image matrix size	128 × 128	152 × 152
In-plane resolution, mm^2	1.5 × 1.5	1.25 × 1.25
Section thickness, mm	4.0	3.0
TR (MS), ms*	12000	12000
TE (SE), ms†	35.5	35.7
TR (STE), ms‡	4.41	4.54
TE (STE), ms§	5.36	5.54
Bandwidth, $Hz \cdot pixel^{-1}$	500	500
No. spokes	35	35
Acquisition time, ms‖	215.75	220.55
Maximum no. sections	55	54
No. averages	1	2
Measurement time, s¶	84	168

*Image repetition time.

†Spin-echo time for $b = 1000\ s \cdot mm^{-2}$.

‡Stimulated echo repetition time.

§Stimulated echo time.

‖Image acquisition time.

¶Total measurement time for multislice DW MRI and 6 diffusion gradient orientations.

STEAM indicates stimulated echo acquisition mode; MRI, magnetic resonance imaging; DWI, diffusion-weighted imaging; TR, repetition time; TE, echo time; MS, multiple slices; SE, spin echo; STE, stimulated echo.

compensation, and the point spread function was calculated as previously described.[10]

Image Reconstruction

Image reconstruction starts by an initial determination of high-quality coil sensitivities from the non-DW data with use of a modified NLINV algorithm and is then followed by a linear inverse reconstruction of all images.

For the first step, an estimate x_{opt} containing the coil sensitivities $c_1, \ldots, c_n$ of n virtual channels and the image content ρ is computed from the measured data y by solving the optimization problem

$$x_{opt} = \arg\min_x \|F(x) - y\|_2^2 + \beta R(x) \text{ with } x = (\rho, c_1, \ldots, c_n).$$

As previously described for real-time MRI,[11] this task is accomplished by the iteratively regularized Gauss-Newton method (IRGNM) with β the regularization parameter of the last IRGNM iteration ($\| \cdot \|_2$ represents the L2 norm). The nonlinear forward operator F contains a multiplication of the image content ρ with the coil sensitivities c_i. With reference to the implementation for real-time MRI, the temporal regularization is replaced by a penalty term $H(c)$, which enforces similarity of the coil sensitivities for directly neighboring sections. Thus,

$$R(x) = \|\rho\|_2^2 + \sum_{i=1}^{n} \|\hat{c}_i\|_2^2 + dH(c)$$

with

$$\hat{c}_i = \left(1 + r\|k\|^2\right)^{l/2} \mathcal{F} c_i$$

and

$$H(c) = \sum_{i=1}^{n} \sum_{j=1}^{s-1} \|\hat{c}_{i,j} - \hat{c}_{i,j+1}\|_2^2.$$

$c_{i,j}$ is the sensitivity of the i-th virtual channel in the j-th section with s the maximum number of sections. The addition of $H(c)$ to the regularization improves the numerical stability for the coil sensitivity estimation with respect to potential phase errors that may arise from local motion (eg, blood flow or brain pulsation). The algorithm was initialized with the following settings

$$\rho_j \sim \sqrt{\sum_{i=1} \left|\mathcal{F}\left(K \cdot Y_{i,j}\right)\right|^2},$$

$$\hat{c}_{i,j} \sim \left(1 + r\|k\|^2\right)^{-l/2} Y_{i,j},$$

$$\|\rho\| = \|\hat{c}\|,$$

and

$$\|Y_{i,j}\| = \|Pj \cdot \mathcal{F}\left(\rho j \cdot c_{i,j}\right)\|.$$

$Y_{i,j}$ represents the gridded k-space data, P_j is the Fourier transform of the point spread function, K is a Gaussian mask used for smoothing,

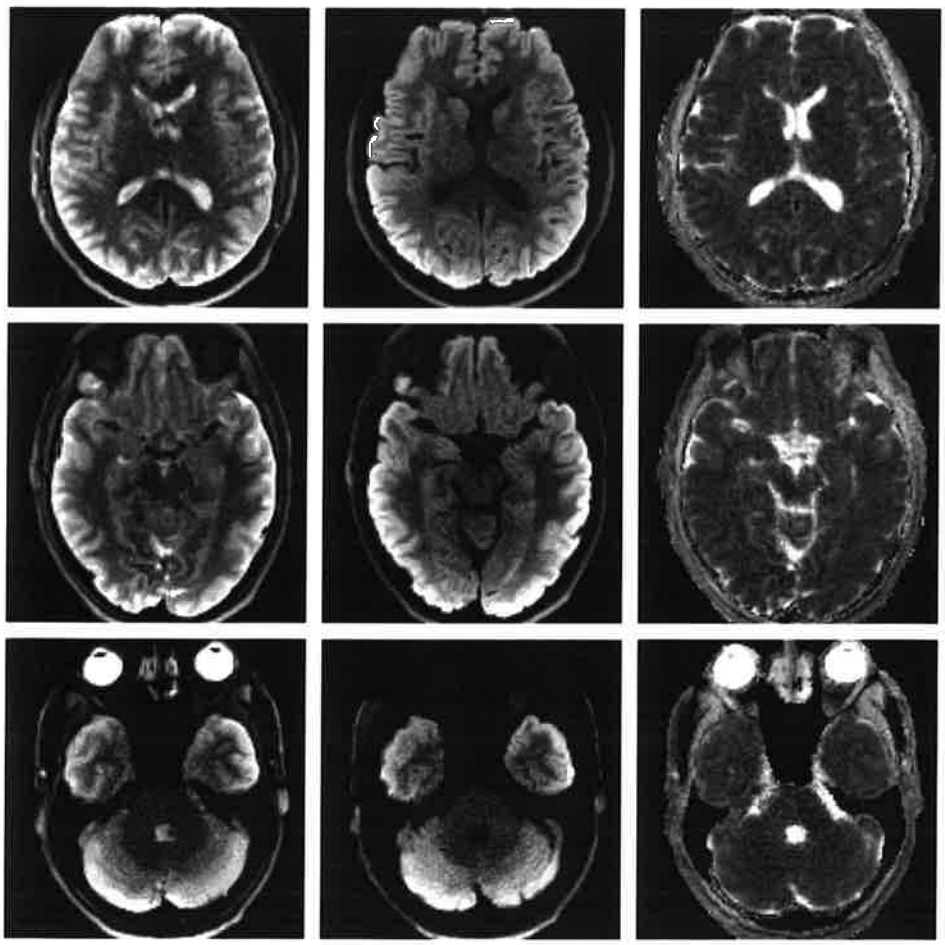

FIGURE 2. Left, Non-DW image; middle, mean DW image; and right, ADC map of the brain of a normal volunteer. The 3 selected sections were obtained by whole-brain DW STEAM MRI and the "fast" protocol (see Table 1).

$\mathcal{F}$ represents the 2-dimensional FFT, and the mid dot denotes pointwise multiplication. The chosen initialization approximates the true phases and magnitudes of the coil sensitivities and therefore leads to fast convergence. The coil sensitivity estimation used $l = 32$, $r = 100$, $d = 1$, and 9 IRGNM iterations.

With known coil sensitivities, the subsequent reconstruction of all images reduces to a linear inverse problem, which is solved with the conjugate gradient method. This is done separately for each image section and diffusion direction.

Postprocessing

Postprocessing included denoising of magnitude images by a modified nonlocal means filter as recently proposed for real-time MRI.[16] The filter was applied to the non-DW images and the mean DW images after averaging. Before exact calculation of the diffusion tensor, the nonlocal means filter was applied to the non-DW image and the 6 DW images for each direction. The ADC maps were multiplied by a binary mask, which sets pixels with intensities below a heuristic threshold in the non-DW image to zero.

Computational Issues

All reconstructions were performed offline after data acquisition. The algorithm was implemented on a single graphics processing unit (GPU) (GeForce GTX TITAN; NVIDIA, Santa Clara, CA) using the MATLAB Parallel Computing Toolbox (R2015b; The MathWorks, Inc, Natick, MA). To save memory on the GPU device, the coil sensitivity estimation was restricted to subsets of slices instead of using the entire data set, that is, 10 slices for the fast DWI protocol and 5 slices for the high-resolution DWI protocol. Reconstruction times for a whole-brain data set were 30 minutes for the fast DWI protocol and 2 hours for the high-resolution DWI protocol, respectively.

RESULTS

Figures 2 and 3 show typical results for the non-DW image, the mean DW image, and the ADC map in 3 selected sections (single subject) for the fast DWI protocol ($1.5 \times 1.5 \times 4.0$ mm^3 in 84 seconds) and the high-resolution DWI protocol ($1.25 \times 1.25 \times 3.0$ mm^3 in 168 seconds), respectively. The achieved image quality was reproducible in all subjects and markedly improved in comparison to a preceding study using DW STEAM MRI with Cartesian encoding and FFT reconstruction.[6] In particular, and in contrast to EPI-based acquisitions, all images from all sections of the brain were free of susceptibility artifacts as assessed by visual inspection. Individual ADC values in the centrum semiovale for all subjects and both DWI protocols are summarized in Table 2. The resulting mean values averaged across subjects of 683 ± 18 (fast DWI) and 680 ± 24 in units of 10^{-6} mm$^2 \cdot$ s^{-1} (high-resolution DWI) are not only identical, but compare well to literature values of 687 ± 23,[17] 703 ± 36,[18] and 736 ± 40.[19]

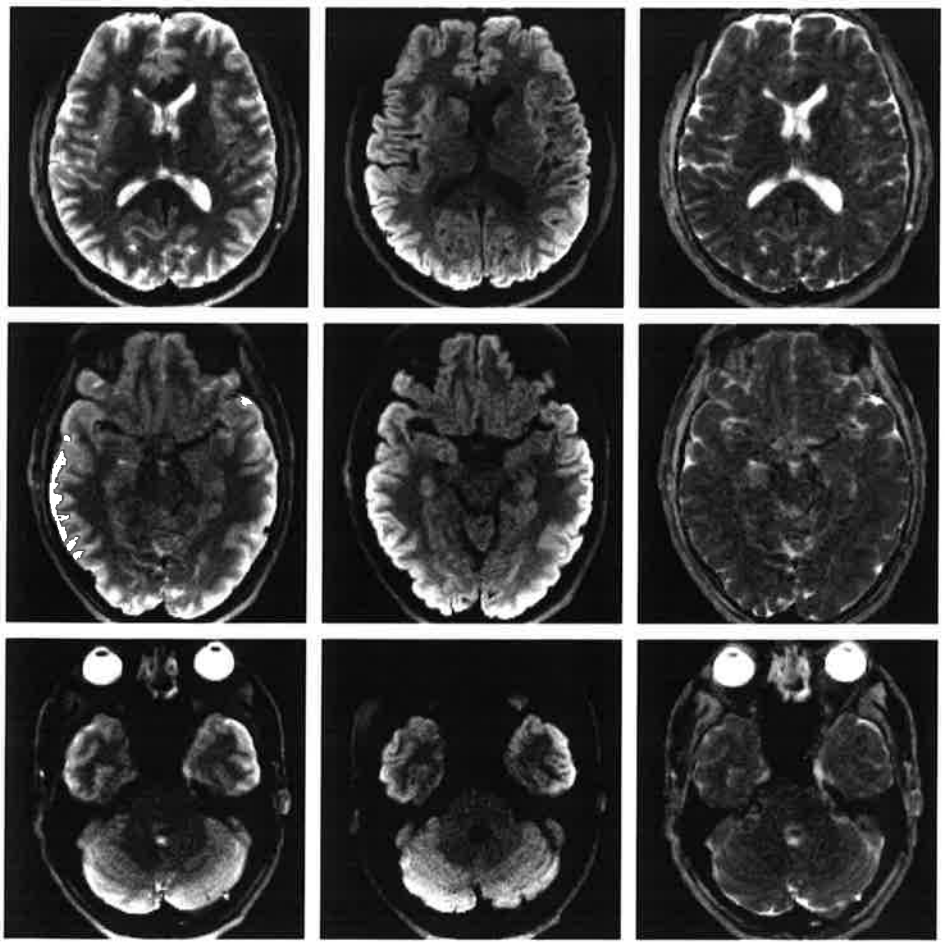

FIGURE 3. Left, Non-DW image; middle, mean DW image; and right, ADC map of the brain of a normal volunteer. The 3 selected sections were obtained by whole-brain DW STEAM MRI and the "high-resolution" protocol (see Table 1).

TABLE 2. ADC Values in the Centrum Semiovale in Units of 10^{-6} mm$^2 \cdot$ s^{-1}

Subject	Fast DWI*	High-Resolution DWI*
#1	680 ± 97	656 ± 82
#2	715 ± 86	682 ± 95
#3	684 ± 79	698 ± 81
#4	665 ± 86	664 ± 94
#5	656 ± 84	645 ± 82
#6	687 ± 73	669 ± 86
#7	673 ± 83	689 ± 78
#8	680 ± 85	709 ± 78
#9	683 ± 75	666 ± 87
#10	708 ± 75	718 ± 82
Mean ± SD†	683 ± 18	680 ± 24

*Mean ± standard deviation within the region of interest.
†Mean ± standard deviation of ADC values across subjects.
ADC indicates apparent coefficient; DWI, diffusion-weighted imaging.

Figure 4 presents non-DW images, mean DW images, and ADC maps for 2 patients in sections central to the lesion. The first patient (Fig. 4, top) initially presented with a left-sided hemiparesis without any sensory symptoms. Magnetic resonance imaging revealed a subacute lacunar stroke in the posterior limb of the right internal capsule. The hindered diffusion in the lesion is best visible in the mean DW image. The slight blurring artifact in the center of the non-DW image close to the ventricles, also visible in the ADC map, is most likely due to flow within the ventricles, which does not affect the DW image. The second patient was admitted to the emergency department because of a 1-time tonic-clonic seizure. Magnetic resonance imaging (Fig. 4, bottom) showed a space-occupying cyst-like lesion in the area of the frontal midline, consistent with the diagnosis of an epidermoid cyst. The mean DW image accurately depicts its location and shape without geometric distortion and is consistent with an internal structure comprising fluid compartments (dark) as well as jelly-like tissue (bright).

DISCUSSION

In a recent comparative study of stroke patients,[6] the presence of susceptibility artifacts in EPI-based DW MRI was shown to complicate the diagnosis in clinical practice. While this problem is avoided for DW STEAM MRI, the latter method was found to be compromised by lower SNR. The main progress of the present work is the development of a modified technique that offers diagnostic image quality in clinically feasible scan times, while retaining the insensitivity to magnetic field inhomogeneity. For example, in comparison to the results obtained by DW STEAM MRI with Cartesian encoding,[6] that is, 25 sections at 10.4 mm^3 resolution (voxel sixe) and 330 seconds measuring time, the current fast DWI protocol offers a 4-fold reduction in measuring time as well as extended volume coverage with twice as many sections, that is, 55 sections at 9.0 mm^3 resolution within 84 seconds. In addition, visual inspection of the DW images shown in Figures 3C, 4C, and 5C from the study of Khalil et al[6] further confirms the current achievements in image quality as characterized by gray/white matter contrast and spatial acuity. Quantitative estimates indicate a 2.5-fold SNR improvement from 36 (single brain section[6]) to 87. Similarly, the high-resolution DWI protocol simultaneously yields a 2-fold smaller voxel size and a 2-fold faster acquisition, that is, 54 sections at 4.7 mm^3 resolution within 168 seconds. These results represent a major advancement in DW STEAM MRI that renders the method an alternative clinical choice to EPI-based DW MRI. This is further confirmed by the preliminary study of 2 patients.

At this stage, the main obstacle to clinical applicability of the novel DW STEAM MRI technique is the high computational demand and corresponding long reconstruction time. However, previous experience with similar problems for real-time MRI indicates that substantial accelerations may be obtained by an implementation of the algorithm on a multi-GPU server integrated into the commercial MRI system.

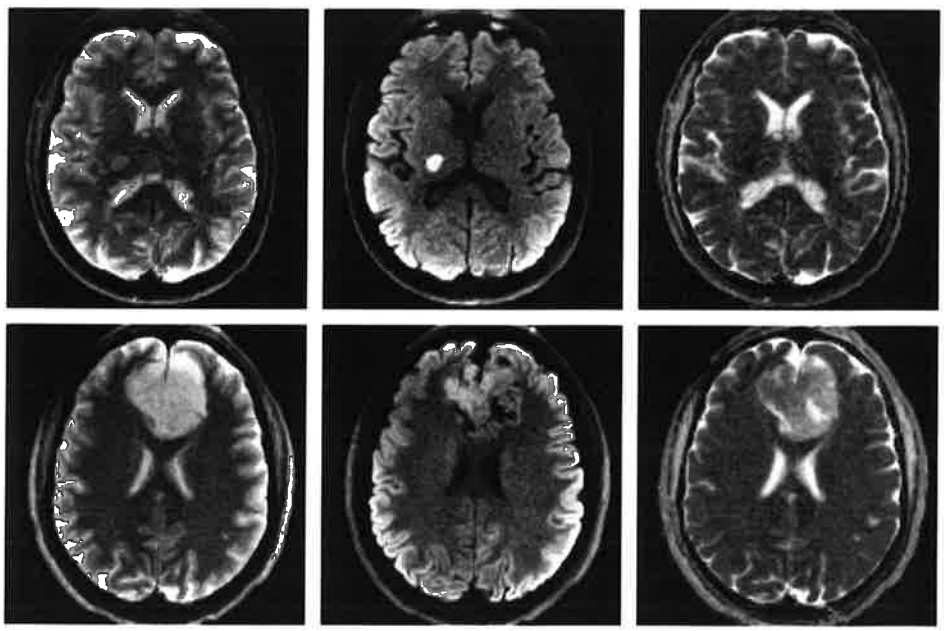

FIGURE 4. Left, Non-DW image; middle, mean DW image; and right, ADC map of the brain of (top) a patient with a diffusion-restricted lesion in the posterior limb of the right internal capsule, consistent with a subacute lacunar stroke, and (bottom) a patient with a frontal diffusion-restricted epidermoid cyst containing fluid compartments (dark in the mean DW image) as well as jelly-like tissue (bright). Experimental parameters as in Fig. 3.

Possible extensions of the current method toward multidirectional diffusion encoding and fiber tractography at higher spatial resolution are straightforward and should be promising in brain regions such as the optic nerve, which are contaminated by air-tissue susceptibility differences.[20] Further advantages are to be expected for organ systems outside the brain, for example, to improve previous DW STEAM MRI studies of the lumbar spine[21,22] or to overcome artifact-prone single-shot EPI-based approaches to DW MRI of the prostate.[23]

In conclusion, undersampled radial STEAM acquisitions with regularized nonlinear inverse reconstruction offers improved DW MRI without susceptibility artifacts. The achievable resolution and image quality allow for rapid whole-brain studies within less than 3 minutes and demonstrate clinical feasibility. While initial patient studies are promising, more widespread clinical applications require accelerated computation and online reconstruction.

ACKNOWLEDGMENT

Dr Sabine Hofer gratefully acknowledges the financial support by the Deutsche Krebshilfe e.V.

REFERENCES

1. Chilla G, Tan C, Xu C, et al. Diffusion weighted magnetic resonance imaging and its recent trend - a survey. *Quant Imaging Med Surg*. 2015;5:407–422.
2. Türkbey B, Aras Ö, Karabulut N, et al. Diffusion-weighted MRI for detecting and monitoring cancer: a review of current applications in body imaging. *Diagn Interv Radiol*. 2012;18:46–59.
3. Le Bihan D, Poupon C, Amadon A, et al. Artifacts and pitfalls in diffusion MRI. *J Magn Reson Imaging*. 2006;24:478–488.
4. Nolte UG, Finsterbusch J, Frahm J. Rapid isotropic diffusion mapping without susceptibility artifacts: whole brain studies using diffusion-weighted single-shot STEAM MR imaging. *Magn Reson Med*. 2000;44:731–736.
5. Rieseberg S, Merboldt KD, Küntzel M, et al. Diffusion tensor imaging using partial Fourier STEAM MRI with projection onto convex subsets reconstruction. *Magn Reson Med*. 2005;54:486–490.
6. Khalil AA, Hohenhaus M, Kunze C, et al. Sensitivity of diffusion-weighted STEAM MRI and EPI-DWI to infratentorial ischemic stroke. *PLoS One*. 2016; 11: e0161416.
7. Frahm J, Haase J, Matthaei D, et al. Rapid NMR imaging using stimulated echoes. *J Magn Reson*. 1985;65:130–135.
8. Frahm J, Hänicke W, Bruhn H, et al. High-speed STEAM MRI of the human heart. *Magn Reson Med*. 1991;22:133–142.
9. Uecker M, Hohage T, Block KT, et al. Image reconstruction by regularized nonlinear inversion—joint estimation of coil sensitivities and image content. *Magn Reson Med*. 2008;60:674–682.
10. Uecker M, Zhang S, Frahm J. Nonlinear inverse reconstruction for real-time MRI of the human heart using undersampled radial FLASH. *Magn Reson Med*. 2010; 63:1456–1462.
11. Uecker M, Zhang S, Voit D, et al. Real-time MRI at a resolution of 20 ms. *NMR Biomed*. 2010;23:986–994.
12. Karaus A, Hofer S, Frahm J. Separation of fiber tracts within the human cingulum bundle using single-shot STEAM DTI. *Open Med Imaging J*. 2009;3:21–27.
13. Block KT, Frahm J. Radial single-shot STEAM MRI. *Magn Reson Med*. 2008;59: 686–691.
14. Haase A, Frahm J, Hänicke W, et al. 1H NMR chemical shift selective (CHESS) imaging. *Phys Med Biol*. 1985;30:341–344.
15. Peters DC, Derbyshire JA, McVeigh ER. Centering the projection reconstruction trajectory: reducing gradient delay errors. *Magn Reson Med*. 2003;50:1–6.
16. Klosowski J, Frahm J. Image Denoising for Real-Time MRI. *Magn Reson Med*. 2016. doi: 10.1002/mrm.26205.
17. Huisman T, Loenneker T, Barta G, et al. Quantitative diffusion tensor MR imaging of the brain: field strength related variance of apparent diffusion coefficient (ADC) and fractional anisotropy (FA) scalars. *Eur Radiol*. 2006;16:1651–1658.
18. Brander A, Kataja A, Saastamoinen A, et al. Diffusion tensor imaging of the brain in a healthy adult population: normative values and measurement reproducibility at 3 T and 1.5 T. *Acta Radiol*. 2010;7:800–807.
19. Hunsche S, Moseley M, Stoeter P, et al. Diffusion-tensor MR imaging at 1.5 and 3.0 T: initial observations. *Radiology*. 2001;221:550–556.
20. Hofer S, Karaus A, Frahm J. Reconstruction and dissection of the entire human visual pathway using diffusion tensor MRI. *Front Neuroanat*. 2010;4:15.
21. Hiepe P, Ros C, Reichenbach J, et al. Diffusion weighted ZOOM imaging in the lumbar spine based on single-shot STEAM. *IFMBE Proceedings*. 2009;25: 670–672.
22. Hiepe P, Herrmann KH, Ros C, et al. Diffusion weighted inner volume imaging of lumbar disks based on turbo-STEAM acquisition. *Z Med Phys*. 2001;21:216–227.
23. Li L, Wang L, Deng M, et al. Feasibility study of 3-T DWI of the prostate: readout-segmented versus single-shot echo-planar imaging. *Am J Roentgenol*. 2015;205:70–76.